Surface & Coatings Technology 204 (2010) 3623–3628

Contents lists available at ScienceDirect

Surface & Coatings Technology

journal homepage: www.elsevier.com/locate/surfcoat

Influences of plasma nitriding edge effect on properties of 316 L stainless steel

M. Olzon-Dionysio [a,*], M. Campos [a], M. Kapp [a], S. de Souza [b], S.D. de Souza [b]

[a] Departamento de Física, Universidade Federal de São Carlos, 13565-950, São Carlos, SP, Brazil
[b] Instituto de Pesquisas Energéticas e Nucleares, 05422-970, São Paulo, SP, Brazil

ARTICLE INFO

Article history:
Received 30 June 2009
Accepted in revised form 13 April 2010
Available online 18 April 2010

Keywords:
316 L stainless steel
Plasma nitriding
Mössbauer spectroscopy
Edge effect
Corrosion

ABSTRACT

Some *rings* of different colors are formed when cylindrical stainless steel samples are plasma nitrided. They appear because of a phenomenon known as the edge effect associated with this technique. In this paper, we discuss some of the characteristics of these *rings* formed in nitrided AISI 316 L austenitic stainless steel: dimension, microhardness, composition, and corrosion resistance. Two cylindrical samples with different diameters were plasma nitrided in a 80% H_2–N_2 gas mixture, at a pressure of about 4 torr, for 4 h, at $T_N = 400$ °C. One of the samples was surrounded by another ring-shaped sample, whose dimensions were chosen to contain the *rings* formed during the nitriding process. Consequently, *rings* of different dimensions were produced. The composition of samples was identified by conversion electron Mössbauer spectroscopy (CEMS) and Glancing angle X-ray diffraction (GAXRD). Regarding their relative dimensions, the *rings* showed similar characteristics, in spite of their different diameters. The samples displayed higher values of hardness in their *rings* than in their central regions. GAXRD detected peaks of Cr_2N on the *rings* and of the expanded austenitic γ_N phase in the central region. CEMS results demonstrated the presence of the paramagnetic γ_N and ε phases. The proportion of these phases was consistent among the samples, regardless of their diameters. Concerning corrosion, the samples with a *ring* showed a poorer corrosion resistance than those without a *ring*. All results are in agreement with the presence of chromium nitride Cr_2N on the *ring* of each sample.

Published by Elsevier B.V.

1. Introduction

Austenitic stainless steels offer good resistance to general corrosion due to the formation of a passive surface film. For this reason, they are widely used in many industrial fields. However, the low hardness and poor tribological properties of these materials can shorten the life of components subject to wear. Some techniques, such as plasma nitriding [1–5], form a surface coating which improves the characteristics of stainless steel components.

Plasma nitriding improves various physical properties of metallic surfaces, such as hardness, wear and corrosion resistance, promoting the use of nitrided samples. This process also has advantages when compared with conventional nitriding processes, for example: non-emission of pollutants, energy saving, and shorter treatment time, despite some inconvenience when components with complex geometry are treated. For instance, plasma nitriding has an associated phenomenon known as the edge effect, which produces a non-uniform surface on cylindrical samples with different colors in the central and peripheral regions. The edge effect occurs because treated samples are submitted to a high cathodic potential to produce plasma directly on their surface. As a result of distortions in the electric field around the corners and edges, the shape of the plasma sheath, which is associated to the shape of samples, determines ion flux distribution, creating erosion rings characterized by different colors and discontinuous hardness. This effect occurs mainly in the treatment of materials containing a high percentage of alloy elements, such as chromium, which produces nitrides, as in the case of AISI 316 L [6,7].

The aim of this research is to investigate the following characteristics of the *rings* formed in nitrided AISI 316 L austenitic stainless steel: dimension, microhardness, composition, and corrosion resistance.

2. Materials and methods

In this study, we used the AISI 316 L stainless steel produced by Villares Metals. Its chemical composition (in wt.%) is: Cr (17.03), Ni (10.16), Mo (2.16), C (0.03), and Fe balance. Three disks, named here samples A, B, and C, and a ring, named sample D, were prepared. Their dimensions are reported in Table 1.

All samples were ground using sandpaper from 220 to 1200 mesh, polished with alumina (0.3 and 1 μm), cleaned ultrasonically in an acetone bath, and finally air-dried. Next, they were plasma nitrided in equipment with d.c. power supply during 4 h. The gas composition was 80% H_2–N_2, at a pressure of about 4 torr. The voltage (~450 V) and current density (~500 mA) were adjusted to maintain the cathode temperature (or nitriding temperature, $T_N = 400$ °C). The

* Corresponding author. Tel./fax: +55 16 3361 4835.
E-mail address: dmod@df.ufscar.br (M. Olzon-Dionysio).

0257-8972/$ – see front matter. Published by Elsevier B.V.
doi:10.1016/j.surfcoat.2010.04.034

Table 1
Sample dimensions (±0.05 mm).

Sample	Diameter	Thickness	Internal diameter	External diameter
A, B, C	19.70	3.90	–	–
D	–	3.90	19.70	31.60

temperature was measured with an alumel–chromel (type K) long rod thermocouple placed underneath the sample.

Sample A was not nitrided to be used for comparison.

Sample D dimensions were chosen to contain the darkest ring formed during the nitriding process, so that sample C, placed inside sample D, could show a uniform color.

This study applied conversion electron Mössbauer spectroscopy (CEMS), X-ray diffraction (XRD), and Glancing angle X-ray diffraction (GAXRD) to identify the phases formed during plasma nitriding.

The Mössbauer spectrometer was calibrated using α-Fe as a reference, operating in a conventional constant acceleration mode, using a backscatter-type gas-flow detector and a 50 mCi nominal activity ^{57}Co(Rh) source. The escape depth of conversion electrons is estimated at about 0.4 to 0.5 μm [8].The detection chamber was self-built, with a 95% He–CH_4 gas mixture flux. Sample analyses were conducted at room temperature and data collected in a multichannel analyser (MCA) to obtain a spectrum of a count rate against source velocity. The amount of each constituent (which contains Fe) in a sample was determined based on the areas under the relevant peaks.

The XRD spectra of untreated and nitrided samples were obtained using a Rigaku (Geigerflex model) diffractometer, Cu Kα radiation (λ = 0.154056 nm). The conditions were: 2θ scan step 0.02°, ranging from 30° to 100°, 2 s counting time. The penetration of conventional X-ray into the sample was ≈3 μm from the surface [9].

The GAXRD spectra of samples B and C were obtained using a Rigaku (Rint-2000) diffractometer, Cu Kα radiation. The conditions were: incident angle fixed at 3°, 2θ scan step 0.02°, ranging from 30° to 45°, 13 s counting time. For this incident angle, the X-ray reaches the thickness of ≈0.6 μm, which is nearly the same as the one probed by the CEMS.

Surface hardness was measured with a Leica microhardness tester (model VMHT-MOT) using a Vickers indenter at a load of 10 g. Hardness was measured at different positions, equally spaced at 0.3 mm apart from each other, aiming at achieving more representative results.

Electrochemical experiments were performed in a conventional Pyrex cell, using untreated (A) and nitrided (B and C) samples as working electrodes (with approximately 0.20 cm^2 of exposed surface area) and a platinum sheet as the counter electrode. Potentials were referred to the saturated calomel electrode (SCE) in a KCl solution. All electrochemical experiments were performed at room temperature and in 3% NaCl aerated electrolytic solution, using Autolab PGSTAT 30 Potentiostat/Galvanostat (Ecochemic, The Netherlands). Potentiodynamic polarization curves were obtained by means of GPES Autolab Software from a cathodic potential ($-1.0\ V_{(SCE)}$) to an anodic potential ($+1.2\ V_{(SCE)}$) at a sweep rate of 1 mV s^{-1}. A microstructural analysis was carried out to evaluate corrosion morphology and the extent of the damage on the surface of untreated and nitrided samples after polarization tests, using a JEOL scanning electron microscope (model JSM-5800 LV). This same equipment was used to measure the thickness of the nitrided layer as well.

3. Results and discussion

Fig. 1 shows pictures of the nitrided samples. An initial visual analysis suggests that regions can be classified according to their color. Thus, the borders of samples B and D, named here as *rings*, are light gray, and were labeled 1 and 4, respectively. Towards the center, there is a region in shades of blue and brown, labeled 2 (sample B) and 5 (sample D). The central region of sample B is dark yellow, labeled as number 3. Sample C, which was nitrided inside ring D shows the same yellow shade and was labeled 6.

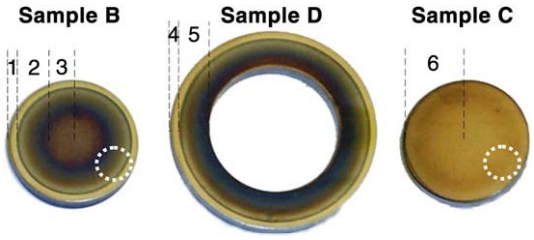

Fig. 1. Visual aspect of nitrided samples, whose different regions are classified according to their distinct colors. Corrosion tests were performed within the white circles.

3.1. Nitrided layer depth and hardness measurements

Fig. 2 (a) and (b) show the Scanning Electron Microscopy (SEM) of a section of the samples B and C to illustrate the measurements of the depth of the nitrided layers.

The arithmetic mean value of 13 different measurements for both samples was done. The depth of sample C is 2.3 ± 0.2 μm. For sample B, two options of depth are possible: the bigger one at the top or the smaller one at the bottom, in Fig. 2 (b). The smallest was chosen (1.5 ± 0.1 μm) because of its consistency with the discussion below.

Regarding the hardness measurements, the arithmetic mean value of 10 measurements on the surface of sample A is 183 ± 27 $HV_{0.01}$.

Fig. 3 depicts hardness values in different regions (numbered 1 to 6, according to Fig. 1) on the surface of the nitrided samples B, C, and D. The mean value for each region is represented by a continuous line. The indent penetration during hardness measurements was between approximately 0.66 μm (region 4) and 1.3 μm (region 2).

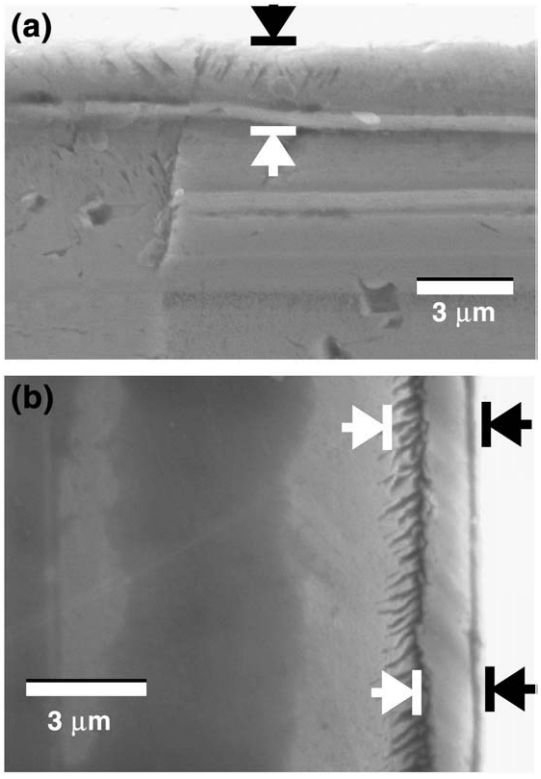

Fig. 2. SEM micrographs of samples C (a) and B (b).

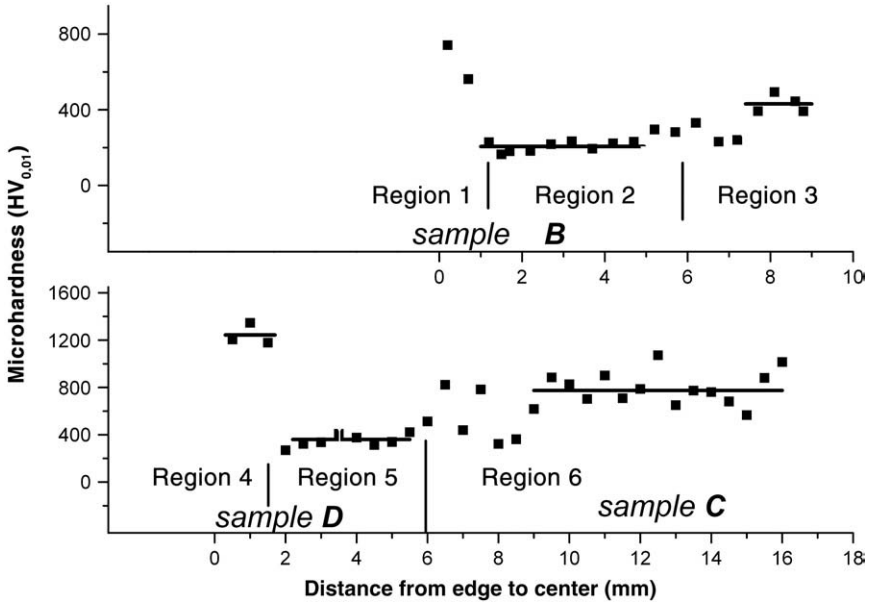

Fig. 3. Hardness in different regions of the nitrided surface of samples B, C, and D.

Treated samples show higher microhardness values when compared with sample A, which was untreated.

Hardness reaches a maximum value in regions 1 and 4, decreasing abruptly in regions 2 and 5. Towards the center of the sample, there is a small interface region after which hardness increases again and tends to stabilize in central regions 3 and 6. This behavior was observed by Alves Jr. et al. as well [6].

Table 2 shows the estimated extension of regions marked in Fig. 1, as well as the arithmetic mean values of hardness in the intervals marked in Fig. 3. The last row displays the hardness values obtained by Alves Jr. et al. [6].

Based on this table, one can see that, despite their different diameters, the extension of equivalent regions in samples B (1 and 4) and D (2 and 5), shown in the fourth row, agree to better than 98%.

Table 3 shows the ratio between the respective hardness values of equivalent regions in samples B, C, and D. These values lack precision, however, compatibility can be observed among them in both situations: sample B and group C + D. As Tables 2 and 3 show, the *rings* formed in samples B and D have the same characteristics. Therefore, *rings* do not seem to depend on sample geometry, at least not in their current dimensions.

It is appropriate to compare the hardness values obtained in our study with those obtained in a similar nitriding gas composition [6]. A gas composition exerts considerable influence on hardness [10], whereas gas pressure practically does not affect it [11]. Although Alves Jr. et al. [6] conducted their study with a smaller sample than the ones used in our investigation, the hardness values they obtained (mentioned in the last row of Table 2) are higher than ours. In a preliminary approach, this seems to contradict our results. However, despite similar gas composition in both studies, Alves Jr. et al. adopted a longer treatment time (5 h) and higher temperature (500 °C). Both variables favor higher hardness values in nitrided layers [12–14].

On the other hand, the hardness value in region 6 is compatible with values measured by other authors, 750 $HV_{0.1}$ [15], who conducted their research under conditions similar to ours, except for pressure, which in their case was of 6 mbar (4.5 torr).

Table 2
Measurements of region extension and mean hardness values for samples B, C, and D.

Position	Border or *ring*		Intermediate		Central	
Sample	B	D	B	D	B	C
Region	1	4	2	5	3	6
Extension (mm)	1.31 ± 0.06	1.33 ± 0.05	4.72 ± 0.08	4.63 ± 0.07	3.82 ± 0.09	9.85 ± 0.08
Mean hardness ($HV_{0.01}$)	652 ± 70	1244 ± 90	206 ± 20	360 ± 30	431 ± 40	775 ± 80
Hardness ($HV_{0.1}$) Ref. [6]	1250		300		500	

3.2. X-ray diffraction (XRD)

Fig. 4 shows the XRD diffractograms of samples A, B, C, and D.

Sample A shows austenitic FCC γ phase peaks. In addition to substrate peaks, samples B, C, and D show broad γ_N phase peaks shifted to lower angles. Probably, peak broadening is a result of nitrogen gradient, residual stresses, and possible defect structure in the nitrided layers [16]. Other possible phases produced during the nitriding process are ε-$Fe_{2+x}N$ (hexagonal) or γ′ (f.c.c.) and chromium nitrides [12,14,17]. Peak positions in each phase are marked below the X-ray diffraction patterns of the samples in Fig. 4.

Comparing the XRD of samples B and C, one can see that:Sample B shows much more γ phase than sample C, indicating that sample B has a thinner nitrided layer than sample C, as was indicated at the bottom of Fig. 2 (b). It also agrees with the smaller value for hardness in region 3 (431 $HV_{0.01}$) compared to region 6 (775 $HV_{0.01}$), as shown in Fig. 3 and Table 2. The γ_N phase of the sample with *ring* (B) is closer to the γ phase than the sample without *ring* (C). It indicates that the γ_N phase presents more N for C than B [18].

Moreover, Fig. 5 shows GAXRD diffractograms of samples B and C. It clearly shows the presence of the Cr_2N phase on the surface of sample B. It explains why the γ_N phase of this sample presents less N than sample C due to the fact that part of the Nitrogen is used to form this Cr_2N phase.

Table 3
Ratio between measured hardness values for equivalent regions in samples B, C, and D.

Equivalent regions in samples B, C, and D.	1 and 2	4 and 5	1 and 3	4 and 6
Ratio between hardness values	3.2 ± 0.7	3.5 ± 0.7	1.5 ± 0.3	1.6 ± 0.4

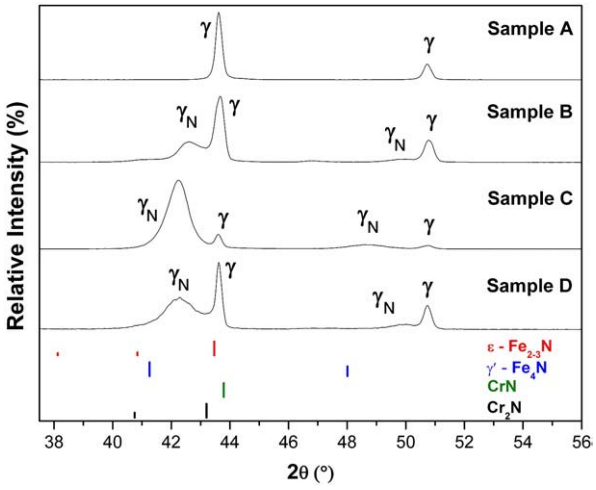

Fig. 4. X-ray diffraction patterns of nitrided samples A, B, C, and D.

The presence of Cr_2N on sample B can also explain the highest values for hardness on the *ring* region, since its hardness value is higher than 1479 HV [19,20]. Moreover, Borgioli et al. [12] suggested that this constituent tends to be concentrated in the outer part of the modified layer. Even though a temperature of 400 °C was used, it possibly exceeded 420 °C in sample borders due to edge effects. At this temperature, the solubility limit of nitrogen in the austenitic structure is reached, the metastable γ_N phase is decomposed, and precipitation of Cr nitrides occurs, which is relatively stable [15,21]. Consequently, the γ_N phase decreases as can be seen in the XRD patterns, Fig. 4, where samples B and D, which contain *rings*, show smaller amounts of γ_N phase than C, without *rings*.

Taking this into account, results for XRD, GAXRD and hardness are consistent and also indicate that there is Cr_2N in the *ring*.

3.3. Conversion electron Mössbauer spectroscopy (CEMS)

Fig. 6 shows CEMS data for samples A, B, C, and D.

The spectra analysis shows that the surface of the untreated sample is represented by parameters IS = −0.09 mm/s and QS = 0.13 mm/s, which means that the austenitic f.c.c. symmetry is affected by the Fe atom neighbors. Besides this substrate spectrum, samples B, C, and D also display the γ_N phase and the hexagonal ε phase ($Fe_{2+x}N$) spectra, with different stoichiometries for the last one.

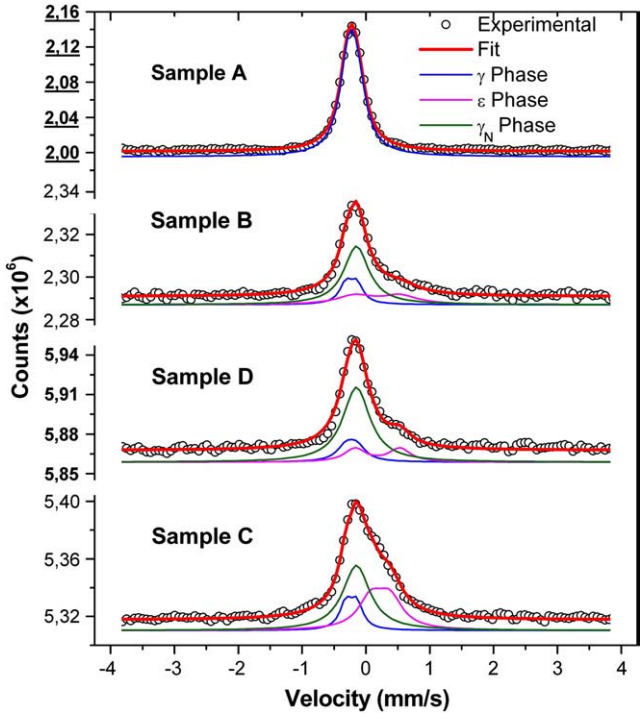

Fig. 6. CEMS data for samples A, B, C, and D.

Table 5 shows the values of hyperfine parameters obtained from the fittings, the quadrupole splitting (QS), the isomer shift (IS), and the relative fraction (RF). These parameters are similar to others published previously, according to the references shown in the right column [22–25].

Regarding the γ phase of the substrate in different samples, one can see that the QS value is higher in the nitrided samples. As this

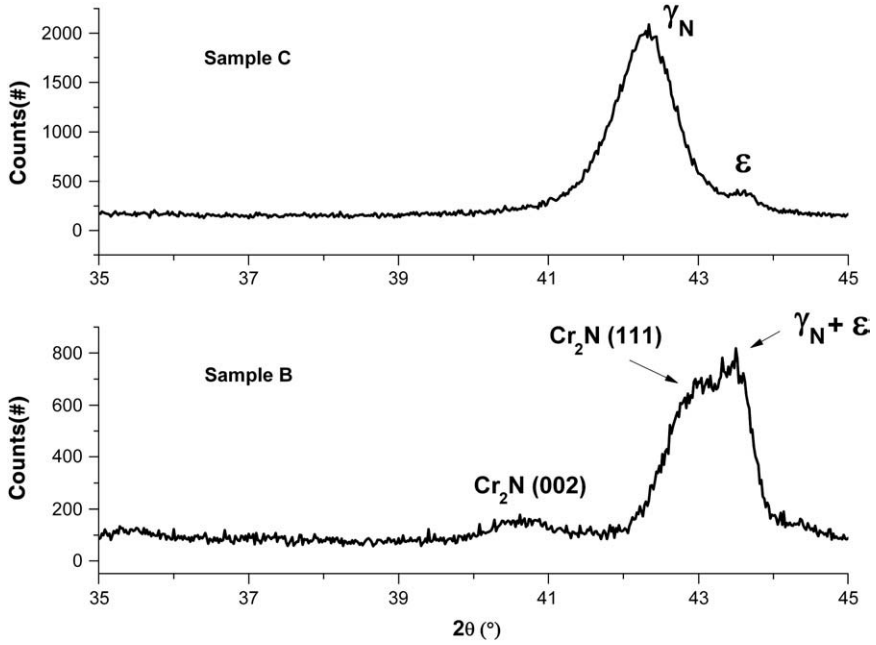

Fig. 5. GAXRD diffraction patterns of samples C (without *ring*) and B (with *ring*).

parameter indicates a decrease in the FCC cubic symmetry caused by the Fe atom neighbors, this higher value of QS can be understood as the production of more Fe atom neighbors by the nitriding process.

The γ_N phase has the magnetic properties of a soft material, which means that it presents the paramagnetic state (singlet in CEMS) for smaller concentrations of N and the magnetic state (six-line pattern in CEMS) for greater concentrations [26].

It is interesting to compare the present results with the previous ones for 316 L [17], where it was observed that the γ_N phase was formed in both states (magnetic and paramagnetic). Here, only the paramagnetic state was observed, indicating less N in this phase. These results are compatible with the X-ray measurements because here (Fig. 4) the first one of the γ_N peaks dislocates less (up to 42°) while the previous dislocation reached up to 40°. Consequently, both current results, XRD and CEMS indicate less concentration for N in the γ_N phase for the present study.

Concerning the ε phase ($Fe_{2+x}N$), depending on the value for *x*, it can show both hyperfine interactions in CEMS: magnetic and paramagnetic (doublet in CEMS). Here we observe only the last one.

To compare the results for samples B and C + D, the values of the relative fraction phase (RF) were normalized on the surface area of this group. These values are represented in the last three rows of Table 4 (16%, 58%, and 26% for γ, γ_N, and ε (or $Fe_{2+x}N$), respectively). These results are compatible with the corresponding values of sample B, which are in agreement with the discussion concerning *ring* based on Tables 2 and 3.

An examination of the sample group C + D reveals that the ε-$Fe_{2+x}N$ phase is concentrated more in the center (38%) than on the border (18.4%). Besides, in the center, the value of *x* is smaller ($x<0.20$) than on the border ($x=0.6$). It means that, proportionally, more N is available in the ε-$Fe_{2+x}N$ phase in the center than on the border. Since the GAXRD results indicated the presence of Cr_2N in the *ring*, the amount of available N in this position is reduced to form the ε-$Fe_{2+x}N$ phase. Therefore, there seems to be some agreement between these results (GAXRD and CEMS) because both suggest the presence of Cr_2N in the *ring*.

3.4. Corrosion behavior

The potentiodynamic polarization curves for nitrided AISI 316 L stainless steel samples A, B, and C are shown in Fig. 7. The corrosion tests were performed in the regions indicated in Fig. 1.

The linear voltammetry of the untreated sample A is also reported as a reference in the same experimental conditions. Both untreated and nitrided samples show the typical corrosion behavior of a passive material subject to pitting corrosion (or localized corrosion). Based on these curves, the corrosion potential (E_{corr}) and the anodic current density (*j*), for potential values $E=0.1$ V, $E=0.5$ V and $E=1.0$ V, are given in Table 5. As can be seen from Table 5, the nitrided sample C (region 6) shows a more positive E_{corr} value than the nitrided sample B (regions 1 and 2). Moreover, the E_{corr} value of the untreated sample is clearly lower when compared with nitrided sample values.

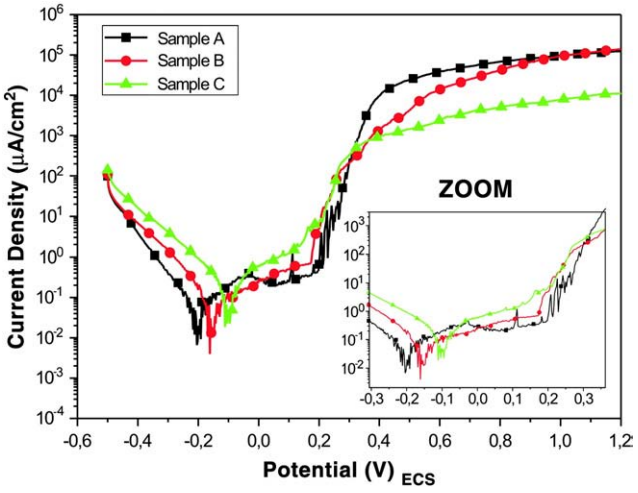

Fig. 7. Potentiodynamic polarization curves of samples A, B, and C in 3% NaCl aerated electrolytic solution.

A passive behavior is observed in sample A, and pitting begins at a potential value of about 0.20 V. With further anodic polarization, the current density increases abruptly at potentials above 0.20 V for this sample, indicating a much higher dissolution than in samples B and C. Therefore, the current density value of about 9.7×10^4 μA cm^{-2} (for $E=1.0$ V) contributes to the development and growth of pits on the surface of sample A. As for sample B (regions 1 and 2), the current density value, for $E=1.0$ V, was $j\approx9.4\times10^4$ μA cm^{-2}, which was very close to the value obtained for sample A at the same potential. As mentioned before, the Cr_2N is present in the *ring*. So, the region (1) does not contain a sufficiently high chromium concentration and it is subject to an active corrosion process [12,27–29].

On the other hand, the current density value (for $E=1.0$ V) obtained for sample C was about 8.0×10^3 μA cm^{-2}, which shows a displacement of the current density towards lower values for this sample, indicating a lower dissolution rate of the pits. This may be due to two factors:

1) The larger concentration of the hexagonal ε ($Fe_{2+x}N$) phase in the center (sample C, 38%) than in the border (sample B, 18.4%), as deduced from the CEMS analysis. As observed by Jirásková et al. [23], the hexagonal ε ($Fe_{2+x}N$) phase can reduce the dissolution rate of pits formed in the presence of aggressive ions.
2) The larger concentration of nitrogen in sample C than in sample B, which facilitates the change of pH, having a neutralizing effect on the acid pits on the corrosion surface [30].

It is interesting to compare the anodic current density (Table 5) of the present results for 316 L with some previous results, obtained for 316 L samples nitrided at 6 mbar (4.5 torr) and under the same conditions of time and temperature [17]. For this comparison, a

Table 4
Hyperfine parameters obtained from the fittings: QS: quadrupole splitting; IS: isomer shift; RF: relative fraction. Typical errors are ±3%.

Sample	Phase	QS (mm/s)	IS (mm/s)	RF (%)	Ref.
A	γ	0.13	−0.09	100	[22]
B	γ	0.17	−0.11	18.7	[22]
	γ_N	0.00	−0.03	56.8	[23]
	ε-$Fe_{2.6}N$	0.70	0.30	24.5	[24]
C	γ	0.17	−0.11	15.8	[22]
	γ_N	0.00	−0.03	46.2	[23]
	ε-$Fe_{2+x}N$ ($x=0.0$; 0.08 or 0.20)	0.30	0.45	38.0	[23,25]
D	γ	0.17	−0.11	16.1	[22]
	γ_N	0.00	−0.03	65.5	[23]
	ε-$Fe_{2.6}N$	0.70	0.30	18.4	[24]
C + D	γ			16.0	
	γ_N			58.0	
	ε-$Fe_{2+x}N$			26.0	

Table 5
Corrosion potential (E_{corr}) and anodic current density (j), for potential values $E=0.1$ V, $E=0.5$ V and $E=1.0$ V, for untreated and nitrided samples.

Samples	E_{corr} ($V_{(SCE)}$)	*j* [for $E=0.1$ $V_{(SCE)}$] (μA cm^{-2})	j [for $E=0.5$ $V_{(SCE)}$] (μA $cm^{-2}\times10^3$)	*j* [for $E=1.0$ $V_{(SCE)}$] (μA $cm^{-2}\times10^4$)
A (untreated)	−0,20	0.24	23.9	9.63
B (with *ring*)	−0,16	0.49	4.23	9.37
C (without *ring*)	−0,11	1.23	1.45	0.78

current density value (for $E = 1.0$ V) was normalized in relation to the untreated sample. Consequently, the ratio $0.78/9.63 = 0.081$ obtained in this study can be compared with the previous ratio $5.7/280 = 0.020$, which is much better than 0.081. Thus, the surface produced at 4.5 torr showed a stronger corrosion resistance than that produced at 4 torr. The highest concentration of nitrogen in the γ_N phase of the previous study [17] can explain this behavior [30].

3.5. Scanning Electron Microscopy (SEM)

Fig. 8 shows the Scanning Electron Microscopy (SEM) of untreated (sample A, Fig. 8a) and nitrided (sample B, regions 1 and 2, Fig. 8b; and sample C, region 6, Fig. 8c) samples of AISI 316 L stainless steel after polarization tests at 3% NaCl aerated electrolytic solution.

These figures illustrate the presence of a larger quantity of pits distributed on the surface of untreated sample A, whereas a smaller quantity of pits is observed in the nitrided sample C (region 6). The *j*/*E* potentiodynamic profile of sample C (region 6) in a medium of aggressive ions of lower current density value (about 0.8×10^4 μA cm^{-2}, for $E = 1.0$ V) shows pits considerably smaller in amount and size than the other samples (Fig. 8 (a) and (b)), as was expected.

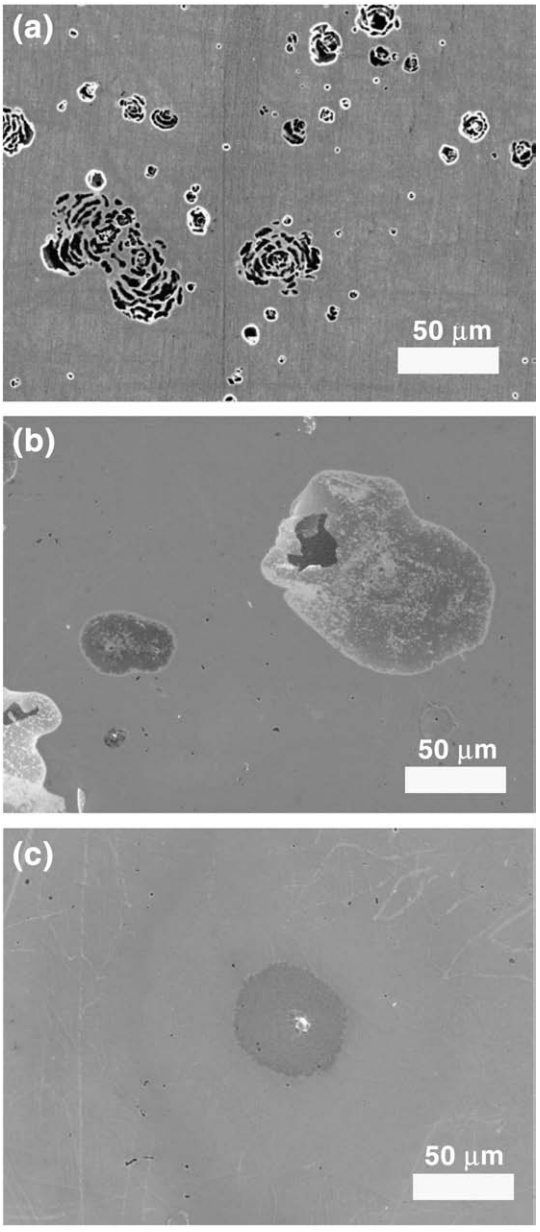

Fig. 8. SEM micrographs of samples A (a), B (b) and C (c) after polarization tests at 3% NaCl aerated electrolytic solution.

4. Conclusion

This paper presents a study of some of the characteristics of the *rings* formed in nitrided AISI 316 L samples, which were prepared with two different diameters. The following conclusions were reached:

(1) Both samples showed the same *ring* characteristics regarding dimensions and hardness.
(2) XRD results showed the γ_N phase. In the *ring*, the N concentration is less than in the central region. Besides this phase, GAXRD also showed the presence of Cr_2N in the *ring*.
(3) CEMS results showed γ_N and ε phases, neither of them in the magnetic state. The normalized fractions of each of the phases are compatible concerning the different regions (border and central) of the samples.
(4) The sample with a *ring* showed poorer corrosion resistance than the sample without it.
(5) All results (corrosion tests, CEMS, XRD, GAXRD, and microhardness) are compatible with the presence of Cr_2N in the *ring*.

Acknowledgment

We thank Dr. J.M.D.A.Rollo, for support in the hardness measurements. We are also grateful to the technical collaborator Natália A. Zanardi. This work was partly supported by the Brazilian research funding agencies CAPES, CNPq and FAPESP.

References

[1] S. Lampman, ASM Handbook, vol. 4, ASM International, Materials Park, OH, USA, 1997, p. 259.
[2] E. Menthe, K.T. Rie, J.W. Schultze, S. Simon, Surf. Coat. Technol. 74–75 (1995) 412.
[3] P.A. Dearnley, A. Namvar, G.G.A. Hibbertand, T. Bell, proc. 1st Conf. on Plasma Surface Engineering, Garmisch-Partenkirchen, 1988, DGM Informationgesellschaft, Oberursel, 1989, p. 219.
[4] A. Turk, C. Bindal, Manuf. Proc. 24 (7) (2009) 898.
[5] M. Keddam, Appl. Surf. Sci. 254 (8) (2008) 2276.
[6] C. Alves Jr., F.O. de Araújo, K.J.B. Ribeiro, J.A.P. da Costa, R.R.M. Sousa, R.S. de Sousa, Surf. Coat.Technol. 201 (2006) 2450.
[7] C. Alves Jr., E.F. Silva, A.E. Martinelli, Surf. Coat.Technol. 139 (1) (2001) 1.
[8] Y. Jirásková, C. Blawert, O. Schneeweiss, Phys. Stat. Sol. (a) 175 (1999) 537.
[9] B.D. Cullity, Elements of X-ray Diffraction, Addison-Wesley, New York, 1960.
[10] E. Menthe, K.T. Rie, Surf. Coat. Technol. 116–119 (1999) 199.
[11] F. Borgioli, A. Fossati, E. Galvanetto, T. Bacci, G. Pradelli, Surf. Coat. Technol. 200 (2006) 5505.
[12] F. Borgioli, A. Fossati, E. Galvanetto, T. Bacci, Surf. Coat. Technol. 200 (2005) 2474.
[13] A. Fossati, F. Borgioli, E. Galvanetto, T. Bacci, Surf. Coat.Technol. 200 (2006) 3511.
[14] B.-Y. Jeong, M.-H. Kim, Surf. Coat. Technol. 137 (2001) 249.
[15] G.-J. Li, Q. Peng, C. Li, Y. Wang, J. Gao, S.-Y. Chen, J. Wang, B.-L. Shen, Surf. Coat. Technol. 202 (2008) 2749.
[16] L. Wang, S. Ji, J. Sun, Surf. Coat. Technol. 200 (2006) 5067.
[17] M. Olzon-Dionysio, S.D. de Souza, R.L.O. Basso, S. de Souza, Surf. Coat. Technol. 202 (2008) 3607.
[18] S. Picard, J.B. Memet, R. Sabot, J.L. Grosseau-Poussard, J.P. Riviere, R. Meilland, Mater. Sci. Eng. A 303 (2001) 163.
[19] Ken Hirota, Yoshihiko Takano, Masaru Yoshinaka, Osamu Yamaguchi, J. Am. Ceram. Soc. 84 (2001) 2120.
[20] S.M. Aouadi, D.M. Schultzea, S.L. Rohdea, K.-C. Wongb, K.A.R. Mitchell, Surf. Coat. Technol. 140 (2001) 269.
[21] C.E. Foerster, F.C. Serbena, S.L.R. da Silva, C.M. Lepienski, C.J. de M. Siqueira, M. Ueda, Nucl. Instrum. Methods Phys. Res., B Beam Interact. Mater. Atoms 257 (2007) 732.
[22] C. Cordier-Robert, L. Bourdeau, T. Magnin, J. Foct, J. Mater. Sci. Lett. 13 (1994) 352.
[23] Y. Jirásková, S. Havlícek, O. Schneeweiss, V. Perina, C. Blawert, J. Magn. Magn. Mater. 234 (2001) 477.
[24] D. Firrao, M. Rosso, G. Principi, R. Frattini, J. Mater. Sci. 17 (1982) 1773.
[25] G.M. Chen, N.K. Jaggl, J.B. Butt, E.B. Yeh, L.H. Schwartz, J. Phys. Chem. 87 (1983) 5326.
[26] O. Öztürk, D.L. Williamson, Surf. Coat. Technol. 158–9 (2002) 288.
[27] A. Shokouhy, M.M. Larijani, M. Ghoranneviss, S.H. Haji Hosseini, G.M. Yari, A.H. Sari, M. Gholipur Shahraki, Thin Solid Films 515 (2006) 571.
[28] A. Fossati, F. Borgioli, E. Galvanetto, T. Bacci, Corros. Sci. 48 (2006) 1513.
[29] J.H. Liang, C.S. Wang, W.F. Tsai, C.F. Ai, Surf. Coat. Technol. 201 (15) (2007) 6638.
[30] H. Baba, T. Kodama, Y. Katada, Corros. Sci. 44 (2002) 2393.